Optical and infrared properties of tetramethyltetraselenafulvalene [(TMTSF)2X] and tetramethyltetrathiafulvalene [(TMTTF)2X] compounds

Jacobsen, Claus Schelde; Tanner, D. B.; Bechgaard, K.

Published in:
Physical Review B

Link to article, DOI:
10.1103/PhysRevB.28.7019

Publication date:
1983

Document Version
Publisher's PDF, also known as Version of record

Optical and infrared properties of tetramethyltetraselenafulvalene [$(TMTSF)_2X$] and tetramethyltetrathiafulvalene [$(TMTTF)_2X$] compounds

C. S. Jacobsen
Physics Laboratory 3, Technical University of Denmark, DK-2800 Lyngby, Denmark

D. B. Tanner
Physics Department, University of Florida, Gainesville, Florida 32611

K. Bechgaard
H. C. Ørsted Institute, DK-2100 Copenhagen, Denmark

(Received 5 July 1983)

The electronic structure of the organic conductors bis-tetramethyltetraselenafulvalene-X [$(TMTSF)_2X$] and bis-tetramethyltetrathiafulvalene-X [$(TMTTF)_2X$] has been investigated by means of polarized optical and infrared reflectance measurements. Analysis of plasma edges in reflectance is used to extract information on transfer integrals. Measurements of infrared reflectance provide information on the energy of charge-transfer processes and on electron-molecular vibration coupling. Far-infrared measurements allow comparison with low-frequency transport properties, and give clues to the transport mechanisms. The main results may be summarized as follows: The $(TMTSF)_2X$ class of materials has chain-axis transfer integrals of order 0.25 eV at 300 K and 0.28 eV at 30 K. The b-axis transfer integral is found to vary from 18 to 24 meV for different X. The $(TMTTF)_2X$ class has a chain-axis transfer integral of the order 0.18—0.20 eV. No b-axis plasma edge is observable. The infrared conductivity spectra of the materials consist of a broad electronic band with superimposed vibrational fine structure. The band is centered at 300 cm^{-1} in the best $(TMTSF)_2X$ conductors and at 2200 cm^{-1} in $(TMTTF)_2PF_6$, an organic conductor of moderate conductivity. The electron-molecular vibration coupling constants for TMTSF and TMTTF appear to be qualitatively similar to those of TTF (tetrathiafulvalene). A new feature is the observation of considerable coupling to modes involving methyl groups, suggesting that a sizable charge density is located near these groups. The electronic band in $(TMTSF)_2PF_6$ sharpens at low temperature, and a pseudogap at 180 cm^{-1} is formed at temperatures above the metal-insulator transition. This behavior is discussed in terms of a possible spin-density-wave contribution to the conductivity. The spin-density-wave amplitude is estimated to be $0.02\mu_B$.

I. INTRODUCTION

Organic conductors based on the donor molecules TMTSF (tetramethyltetraselenafulvalene) and TMTTF (tetramethyltetrathiafulvalene) combined in a 2:1 ratio with various monovalent, inorganic ions (such as PF_6^-, AsF_6^-, ClO_4^-, ReO_4^-, Br^-, etc.) are of great current interest.[1,2] The TMTSF group comprises mostly good organic metals, typically with conductivities $\sigma(300\text{ K})=600\ \Omega^{-1}\text{cm}^{-1}$, and $\sigma(T)\sim T^{-2}$ (Ref. 3). Observed ground states include superconductivity[4,5] ($T_c\cong 1$ K, ambient or small hydrostatic pressure), antiferromagnetism,[6–8] and nonmagnetic insulators.[9] The TMTTF group contains generally organic metals in the intermediate class [$\sigma(300\text{ K})=1-100\ \Omega^{-1}\text{cm}^{-1}$] with broad conductivity maxima and semiconducting behavior at low temperatures.[10] The application of high pressure induces metallic behavior[11] and makes the materials look more like the selenium analogs, although superconductivity has not been safely identified. In both classes it is found that counterions with lower than octahedral symmetry often perturb the electronic properties through order-disorder transformations, which change the crystal symmetry.[12]

Several features are identical for all materials in the two groups. Most important are the crystal structure and the band filling. The triclinic unit cell[13,14] contains one anion and two donor molecules with a slipped overlap, qualitatively like that of the TTF stack in TTF-TCNQ (tetrathiafulvalene-tetracyanoquinodimethane).[15] However, in contrast to TTF-TCNQ, the stacking axis (a) is almost normal to the molecular plane, resulting in a zigzag type of stack. Neighbor stacks interact through short intermolecular separations forming sheets of molecular stacks (along the b axis) alternating with sheets of anions (along the c axis). Thus a highly anisotropic band structure results.

The basic one-electron, one-dimensional band structure is sketched in Fig. 1. The conduction band is a half-filled hole band. The small gap at the zone edge follows from a small dimerization associated with the zigzag structure. The size of this gap (as estimated from intermolecular distances) is normally assumed to vary strongly from material to material and may have implications for superconductivity, etc.[16]

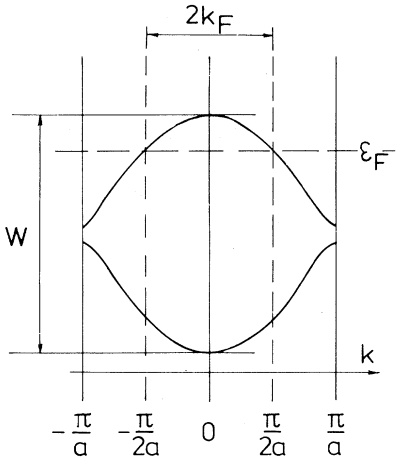

FIG. 1. One-electron, one-dimensional band structure of $(TMTSF)_2X$ and $(TMTTF)_2X$ in the stacking direction. Note that the lattice constant a comprises two organic molecules.

Attractive features which make physical interpretation simpler include the presence of one kind of stack only, the virtual absence of mixing between excitations in the molecular plane and excitations in the stacking direction (except for the anomalous vibrational features discussed below), and a charge density given by stoichiometry.

The purpose of the present paper is to describe experiments on optical and infrared properties, which we have made over the last few years. We shall discuss the implications of these studies for band structure, electron-molecular-vibration (emv) coupling, phase transitions, and conductivity mechanism. Preliminary results have previously been reported in Refs. 17 and 18. Related to our work has been the studies by Kikuchi *et al.*[19] on the overall optical properties of $(TMTSF)_2ClO_4$, the work on vibrational assignments and emv coupling by Bozio and co-workers,[20,21] and far-infrared investigations on $(TMTSF)_2ClO_4$ by Ng *et al.*[22,23] and Challener *et al.*[24] Helberg[25] has conducted studies concerning the orientation of the principal axes in the visible range.

The plan of the paper is the following. First, we discuss experimental procedures. Next, we address the electronic structure of these materials for a, b, and c polarizations. We then describe in some detail the signatures of emv coupling and the distribution of oscillator strength in the chain-axis direction. For the single case $[(TMTSF)_2PF_6]$ where far-infrared spectra have been obtained, we give a detailed analysis of the data and discuss our results in relation to the dc transport properties.

II. EXPERIMENTAL

Single crystals of the materials were prepared electrochemically as described elsewhere.[3] Microanalysis showed 2:1 stoichiometry within experimental limits (0.5%). All samples were elongated in the a-axis direction and had most often reasonable quality (001) faces. Measurements have been done for the electric field along the stacking a-axis direction, and along the b' axis, which designates the direction in the a-b plane, which is perpendicular to the a axis. A few samples have been investigated in unidentified faces in directions approximately perpendicular to a and b'.

In a triclinic crystal nothing can be said *a priori* about the optical axes. However, the observed conductivity anisotropies[3] suggest that a and b' are principal axes at low frequencies, where charge-transfer excitations dominate, i.e., in the infrared range. Helberg[25] has found that a is a principal axis through the visible as well, although the other axes rotate in this range. Thus the measured b'-axis spectra are not representative of a principal axis in the entire frequency range.

Owing to the opaque nature of the crystals, all measurements were done as reflectance. As reflectance standard we used evaporated gold or aluminum giving an accuracy of order 1% on the absolute value.

Various instruments were employed. The far infrared (10—700 cm^{-1}) was covered with a Michelson interferometer, combined with a wire grid polarizer and a cooled bolometer detector. Two Perkin-Elmer grating monochromators (PE-16U and PE-98) provided radiation in the (350—20 000)-cm^{-1} range. Some measurements in the (5000—30 000)-cm^{-1} range were done with a fused quartz prism monochromator (PE-98). A Perkin-Elmer polarizer (gold grid on AgBr) was used from 350—5000 cm^{-1}, while Glan-Thompson prisms and plastic (dichroic) polarizers were used at higher frequencies. A variety of detectors has been employed including thermocouples, PbS cells, Golay cells, and photomultipliers. As radiation sources, a mercury arc, a Globar, a tungsten filament lamp, and a xenon high-pressure arc have been used for the far infrared, intermediate infrared, near infrared, and visible to near ultraviolet, respectively.

Most measurements were done on single crystals, a few mm long and up to 0.5 mm wide. However, for far-infrared and in some cases intermediate-infrared measurements, mosaics of optically aligned crystals were constructed to ensure an acceptable S/N ratio. After the primary reflectance measurements these mosaics were covered with gold and the measurements repeated. In this way the effective filling factor of the mosaic can be reliably estimated, and simultaneously undesired diffraction or interference effects of the mosaic are revealed. Such effects were only observed in the very far infrared, for $\vec{E}||b'$, where the small crystal dimension is comparable to the wavelength of the radiation. In the data presentation, it has been assumed that the gold-covered mosaic provides a usable reference spectrum.

Low-temperature spectra were obtained by thermally anchoring the sample to a controlled cold finger. Radiation shields with suitable holes were used. However, in all cases a considerable amount of 300-K radiation was absorbed in the sample. To estimate the actual sample temperature, a TTF-TCNQ crystal was placed in the sample position, and the well-known resistivity versus temperature of this material[26] was used as a calibration. The reflectance and absorbance properties of TTF-TCNQ (Ref. 27) are quite comparable to those of the $(TMTSF)_2X$ materials in the range of 300-K radiation. It has been found that with the mounting technique employed sample temperatures cannot be lowered below about 25 K.

III. ELECTRONIC STRUCTURE OF THESE COMPOUNDS

In Fig. 2 is presented typical near-infrared—visible-reflectance spectra of $(TMTSF)_2AsF_6$ and $(TMTTF)_2PF_6$ taken at 300 K for polarizations along a and b'. The broad features are identical to those found in many other organic conductors, as, for example, TTF-TCNQ (Ref. 28): The stacking direction (a) displays a sharp drop in the near infrared with a minimum at 8000 and 7600 cm^{-1} for the two materials, respectively. The position agrees with earlier studies on $(TMTSF)_2PF_6$,[17] $(TMTSF)_2ClO_4$,[19] and on polycrystalline samples of the $(TMTTF)_2X$ salts.[10] This reflectance edge is associated with the plasma behavior of the conduction electrons. From the minimum and up through the visible no transitions can be identified. In contrast, TTF-TCNQ displays a number of bands for polarization along the chain axis.[28]

A. Molecular excitations in the transverse direction

For $\vec{E}||b'$ the reflectance is low and rather dispersionless throughout the range: Here the materials are highly anisotropic. In the visible at least two absorption bands can be seen. In $(TMTTF)_2PF_6$ there is a band at 17 000 cm^{-1} and a shoulder at 22 000 cm^{-1}. The bands in $(TMTSF)_2X$ can be seen more clearly in Fig. 3(a), where two polarizations perpendicular to the chain axis in $(TMTSF)_2SbF_6$ are shown, and in Fig. 3(b) where the temperature dependence for $(TMTSF)_2AsF_6$ along b' is presented. There are two distinct absorption bands at approximately 15 000 and 18 000 cm^{-1} and a rise towards another band above 25 000 cm^{-1}. There may be a weak band near 10 000 cm^{-1}. Similar bands were found by Kikuchi *et al.*[19] in $(TMTSF)_2ClO_4$ (b') and must therefore be characteristic for the TMTSF stacks.

An interesting feature is that the 18 000-cm^{-1} band is strongest in the b' polarization, while the 15 000-cm^{-1} band is strongest in the other polarization. The long axis of the TMTSF molecule is about 65° off the b' axis.[13] Thus it appears that the 15 000-cm^{-1} transition is polarized along the long axis of the TMTSF molecule, while the 18 000-cm^{-1} band is polarized along the short axis. The main effect of lowering the temperature is a sharpening of the bands.

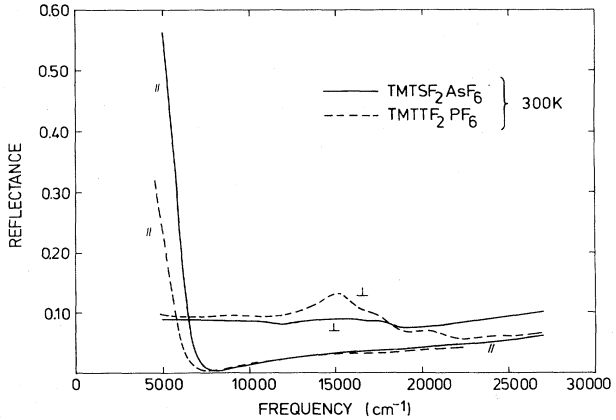

FIG. 2. Polarized room-temperature reflectance of $(TMTSF)_2AsF_6$ and $(TMTTF)_2PF_6$ from 5000 to 27 000 cm^{-1}. The stacking axis a corresponds to ||, while ⊥ is the b' direction.

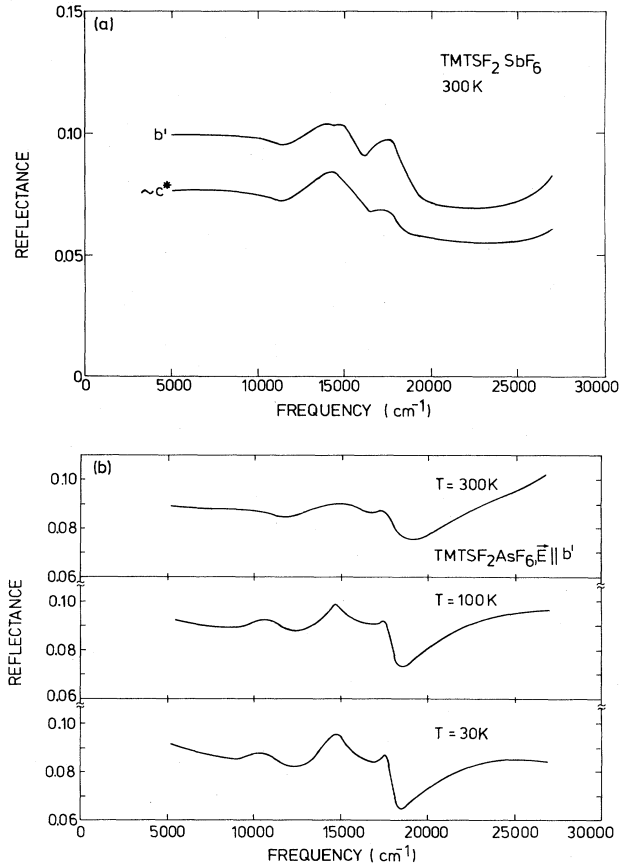

FIG. 3. Polarized reflectance of $(TMTSF)_2X$ perpendicular to chain axis. (a) $(TMTSF)_2SbF_6$ for two different polarizations at $T=300$ K, and (b) $(TMTSF)_2AsF_6$ for $\vec{E}||b'$ at $T=300$, 100, and 30 K. The frequency range is 5000—27 000 cm^{-1}.

According to the work by Zahradnik *et al.*[29] on TTF^+ and by Gleiter *et al.*[30] on the neutral molecules, the conduction electron resides in a b_{1u} orbital with lowest allowed transitions to and from b_{2g} and b_{3g} orbitals. Solution spectra indicate the presence of a weak absorption band at lower energy than the others, tentatively identified as a forbidden $b_{1u} \rightarrow a_u$ transition allowed by vibronic coupling. If the 10 000-cm^{-1} band is real, it may be due to the latter transition, and thus opens the possibility of an excited level about 1.2 eV from the bottom of the conduction band. This is comparable to the one-electron bandwidth estimated below. The 15 000-cm^{-1} excitation should then be to or from a b_{3g} level, while the 18 000-cm^{-1} band corresponds to a transition to or from a b_{2g} level. These assignments are based on the observed polarizations.[30]

We note that the spectrum is qualitatively different from those of $(TMTTF)_2PF_6$ (presented here), $(TMTTF)Br_x$,[31] and $(TSF)Br_x$,[31] which all show a strong

band in (15 000—18 000)-cm^{-1} range and a weak shoulder at 22 000 cm^{-1}. Thus it is conceivable that the electronic structure of TMTSF may deviate in a qualitative way from other tetrachalcogenafulvalenes. This point deserves further clarification.

B. Chain-axis transfer integral

Returning now to the chain-axis polarization, the absence of bands in the visible is a clear consequence of the orientation of the molecules. The transition dipoles of low-lying intramolecular transitions are close to perpendicular to the stacking axis. However, any charge-transfer excitation along the stack would be observed. It seems that there is only one such charge-transfer band, i.e., that associated with the plasma edge. There is no sign of localized excitations corresponding to double occupancy on TMTSF molecules (the so-called U band). Such excitations are seen in several TTF halides,[31] but may be expected to be very weak when the carrier density is low.[32]

In Fig. 4 we show the temperature dependence of the $\vec{E}||a$ spectrum of $(TMTSF)_2AsF_6$. The only significant change is a small blue shift ($\cong$500 cm^{-1}) of the plasma edge on cooling. A similar shift has been observed in $(TMTSF)_2ClO_4$ by Kikuchi *et al.*,[19] and is quite similar to the shift of the edge in TTF-TCNQ.[33] The shift may be associated with thermal contraction, which results in an increase in bandwidth.

The near-infrared chain-axis reflectance of organic conductors is customarily analyzed in terms of the Drude model for the dielectric function:

$$\tilde{\epsilon}(\omega)=\epsilon_\infty-\frac{\omega_p^2}{\omega(\omega+i\Gamma)} . \tag{1}$$

ω_p is the bare plasma frequency, ϵ_∞ is the background dielectric constant, and Γ is a relaxation rate. This model is indeed found to represent the TMTTF and TMTSF materials very well in the vicinity of the plasma edge, in part because unlike the TCNQ salts, there are no absorption bands near the edge to take into account.

Assuming a one-electron band, ω_p is given by[34]

$$\omega_p^2=(e^2/\hbar^2\epsilon_0)\sum_{\mathrm{BZ}}\left[\frac{\partial^2\epsilon_k}{\partial k_\mu^2}\right]f(\epsilon_k) , \tag{2}$$

where BZ represents the Brillouin zone, $f(\epsilon_k)$ is the Fermi-Dirac occupation number, and $\partial^2\epsilon_k/\partial k_\mu^2$ indicates a derivative along the polarization of the electric field. For a one-dimensional tight-binding band with transfer integral t, intermolecular spacing d, volume per molecule V_m, and number of carriers per molecule ρ, Eq. (2) yields (at $T=0$)

$$\omega_p^2=\frac{4td^2e^2}{\pi\epsilon_0\hbar^2V_m}\sin\left[\frac{\pi\rho}{2}\right] . \tag{3}$$

Here $d=a/2$ and $\rho=0.5$. Thus the dimerization associated with the zigzag structure is neglected, making the resulting transfer integral an average value.

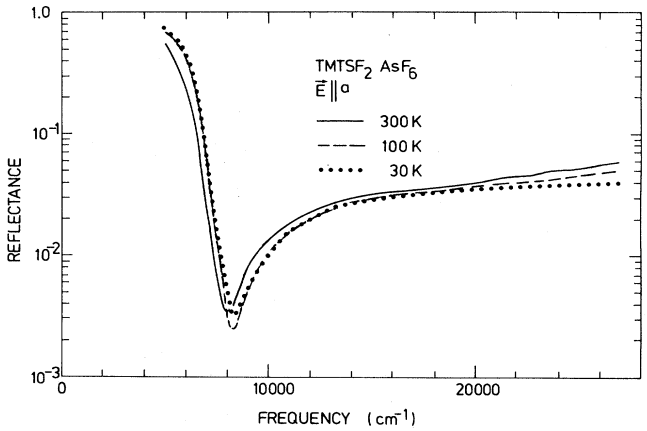

FIG. 4. Chain-axis reflectance of $(TMTSF)_2AsF_6$ at $T=300$, 100, and 30 K. The frequency range is 5000—27 000 cm^{-1}. Notice the logarithmic reflectance scale.

Table I gives Drude parameters and transfer integrals for $(TMTSF)_2AsF_6$ at three temperatures, and for $(TMTSF)_2PF_6$ and $(TMTTF)_2PF_6$ at room temperature. The Drude parameters have been obtained by fitting Eq. (1) to the logarithm of reflectance. In this way the plasma minimum and the low values of reflectance above the edge are well reproduced, ensuring a precise determination of ω_p and ϵ_∞. The results for $(TMTSF)_2AsF_6$ and $(TMTSF)_2PF_6$ compares very well with those reported by Kikuchi *et al.*[19] on $(TMTSF)_2ClO_4$. Other materials like $(TMTSF)_2SbF_6$ and $(TMTSF)_2ReO_4$ are found to have very similar edge positions. Thus it appears that the whole $(TMTSF)_2X$ group has nearly the same $\omega_p=9900$ cm$^{-1}\pm2\%$ at room temperature, with a 5% increase on cooling. In TTF-TCNQ ω_p increases about 10% on cooling,[33] but this is partly due to a change in carrier density. Eliminating this carrier density change the shifts are almost identical.

Estimates of transfer integrals based on Eq. (3) are generally found to be reliable for highly conducting organic salts in the sense that they vary consistently with expecta-

TABLE I. Drude parameters and transfer integrals for the chain axis.

Material	T (K)	ϵ_∞	ω_p (cm^{-1})	Γ (cm^{-1})	t_a (eV)
$(TMTSF)_2AsF_6$	300	2.56	9 940	1230	0.25
$(TMTSF)_2AsF_6$	100	2.52	10 270	1030	0.27
$(TMTSF)_2AsF_6$	30	2.55	10 470	1160	0.28
$(TMTSF)_2PF_6$	300	2.42	9 700	1520	0.25
$(TMTTF)_2PF_6$	300	2.50	8 860	1380	0.20

tions from material to material,[31] with varying temperature,[33] and so forth. The value found for $(TMTSF)_2X$, $t_a \cong 0.25$ eV at room temperature, is surprisingly large. However, estimates of this quantity based on thermoelectric power, which depends on both the band structure and the details in the scattering mechanism, give $t_a \cong 0.35$ eV, assuming acoustic one-phonon scattering.[35] Also a recent reanalysis of TMTSF-DMTCNQ (dimethyltetracyanoquinodimethane),[36] yields $t \cong 0.25$ eV for the TMTSF stack. This stack is regular, with a slipped overlap almost identical to that in $(TMTSF)_2X$.

A relevant material for comparison is TSF-TCNQ. TSF (tetraselenafulvalene) is the parent molecule of TMTSF (i.e., with no methyl groups). The overlap pattern of TSF molecules in TSF-TCNQ (Ref. 37) is similar to that of TMTSF in $(TMTSF)_2X$. The interplanar distances are 3.52 and 3.65 Å, respectively. Thus if the methyl groups had no drastic effects on the orbital, the TSF stack would be expected to have a slightly larger t than a TMTSF stack. In contrast, Welber *et al.*[38] find $t=0.15$ eV for the TSF stack. Although this value depends on an estimate for the TCNQ stack in this material, to make it much larger would be inconsistent with the data. The main conclusion of this discussion is that the attached methyl groups do indeed significantly perturb the highest occupied molecular orbital in TMTSF in a way to enhance the stacking overlap. Molecular vibration studies (see below) indicate that charge may be displaced towards the methyl groups.

The results for $(TMTTF)_2PF_6$ given in Table I should be regarded with reservation. The material is not highly conducting [$\sigma(300\ \text{K}) \simeq 20\ \Omega^{-1}\text{cm}^{-1}$].[10] Also infrared measurements, reported below, indicate that the charge-transfer band is centered around 2200 cm^{-1}, which is not vanishing compared to ω_p. Fitting to a Drude-Lorentz model

$$\tilde{\epsilon}(\omega)=\epsilon_\infty-\frac{\omega_p^2}{(\omega^2-\omega_{\text{CT}}^2)+i\omega\Gamma}\ , \tag{4}$$

where $\hbar\omega_{\text{CT}}$ is the energy of the dominant charge-transfer excitation, yields $\omega_p \cong 8600$ cm^{-1}, which with the model of Eq. (3) gives $t \simeq 0.18$ eV. However, this model is difficult to reconcile with a low dc conductivity and a charge-transfer band at such a high frequency. So a considerable uncertainity in the estimate of t for $(TMTTF)_2X$ remains.

C. Transfer integral perpendicular to chain axis

In this section we present and discuss data relevant to the so-called transverse plasma edge in $(TMTSF)_2X$.[17,18] Figure 5 gives the b'-axis reflectance of $(TMTSF)_2PF_6$ at 300 and 25 K from 0 to 1800 cm^{-1}. At 300 K, R drops rapidly from unity and becomes rather flat above 500 cm^{-1}. The peaks at 560 and 835 cm^{-1} are due to vibrational modes in the PF_6^- ion.[39] At 25 K the overall reflectance remains rather high up to 700 cm^{-1}, while it drops rapidly to low values on the high side of the split PF_6^- bands. The rise in reflectance occurs gradually with cooling; there is no indication of a sudden transition. A minimum is located around 1200—1400 cm^{-1}, while at higher frequencies R reaches a level of about 9% with no significant structure until the visible. In addition to these overall features, there is considerable vibrational fine structure in the far infrared.

We understand this behavior as arising from metallic properties in the b' direction: At 300 K the plasma edge is overdamped, while at 25 K it is reasonably sharp, although with a lot of superimposed features from molecular vibrations. Figure 6 presents the corresponding frequency-dependent conductivity as obtained from dispersion analysis.[34] As expected $\sigma_b(\omega)$ is rather flat at room temperature. The extrapolated dc level is about 20 $\Omega^{-1}\text{cm}^{-1}$, a bit higher than the reported[40] value of 4 $\Omega^{-1}\text{cm}^{-1}$. At 25 K $\sigma_b(\omega)$ rises below 1000 cm^{-1}, reaching a level near dc of 140 $\Omega^{-1}\text{cm}^{-1}$, again larger than the dc conductivity,[40] which is 30 $\Omega^{-1}\text{cm}^{-1}$. It seems conceivable that the dc conductivity is inhibited by macroscopic defects.

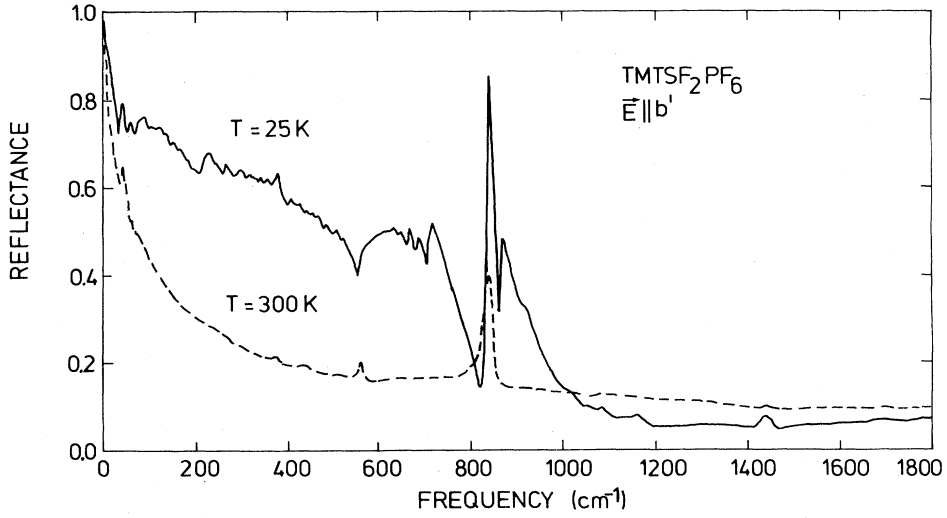

FIG. 5. Polarized reflectance for $\vec{E}||b'$ of $(TMTSF)_2PF_6$ at $T=25$ and 300 K. The frequency range is 10—1800 cm^{-1}.

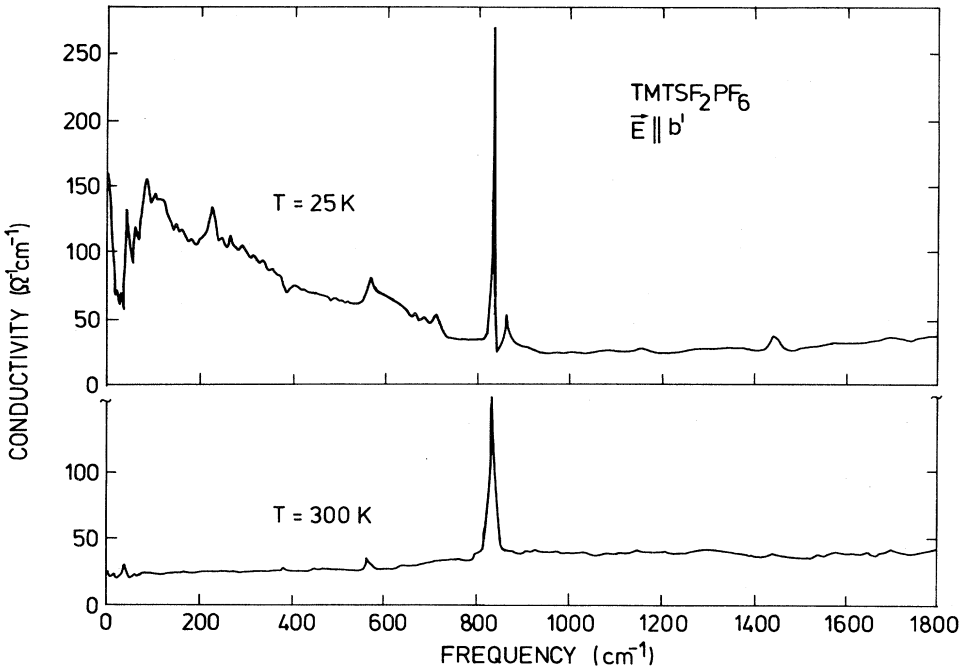

FIG. 6. Frequency-dependent conductivity of $(TMTSF)_2PF_6$ for $\vec{E}||b'$, as obtained by dispersion analysis of reflectance data. Data are given for $T=25$ and 300 K in the frequency range 10—1800 cm^{-1}.

At both 25 and 300 K we note that most of the vibrational lines appear as superimposed bands with no clear evidence for coupling effects. One exception may be the dip in $\sigma_b(\omega)$ below 100 cm^{-1} at 25 K. Apart from this, there is no evidence for a gap along b'. In order to verify the interpretation of the b'-axis spectra, we have performed a series of measurements on other materials.

Figure 7 shows the b'-axis reflectance for $(TMTTF)_2PF_6$ at 300 and 30 K in the range 600—1500 cm^{-1}. The only spectral feature is the 835-cm^{-1} PF_6^- line; there is no rise in reflectance level as temperature is lowered. A similar check has been done on $(TMTTF)_2Br$, which is the best metal in the TMTTF group, down to 300 cm^{-1}; again no sign of metallic behavior is seen. These data show that the high b'-axis reflectance level in $(TMTSF)_2PF_6$ occurs only for the TMTSF chain system. Inspection of the crystal structure[13] suggests that the plasma edge is associated with transfer of charge from TMTSF stack to neighbor TMTSF stack. The transfer is mediated by a rather high transfer integral. A change in the donor molecule from selenium to sulfur apparently diminishes the transfer integral considerably, so that the rise in reflectance is unobservable in the measured range.

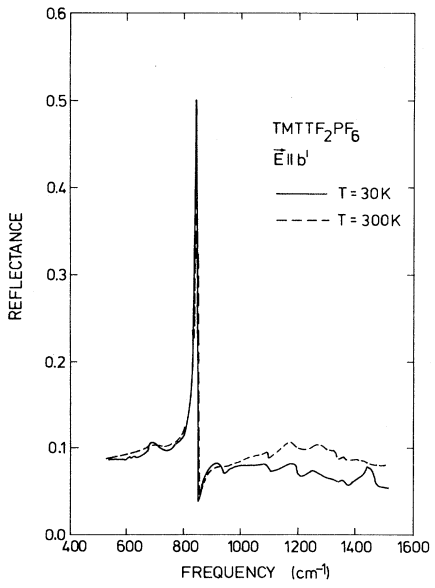

FIG. 7. Polarized reflectance for $\vec{E}||b'$ of $(TMTTF)_2PF_6$ at $T=30$ and 300 K. The frequency range is 500—1500 cm^{-1}.

In the third crystallographic direction the transfer integral should be negligible and no rise in R is expected. Figure 8 shows the low-temperature reflectance of $(TMTSF)_2AsF_6$ along b' and along the direction, which is approximately perpendicular to a and b'. Clearly no edge is seen in this third direction, the main feature again being a counterion absorption line.[39]

As final examples we show in Fig. 9 the b'-axis edges in $(TMTSF)_2SbF_6$ and $(TMTSF)_2ClO_4$. The 300-K b-axis lattice constant in $(TMTSF)_2SbF_6$ is[41] 7.728 Å, while in $(TMTSF)_2ClO_4$ it is[42] 7.678 Å. The latter material has one of the most dense packings in the family, and it appears from Fig. 9 that this packing results in a significant blue shift of the transverse plasma edge, as might be expected.

For more quantitative estimates we have fitted the Drude model of Eq. (1) to the low-temperature edges of different materials. The sharp anion lines are modeled by

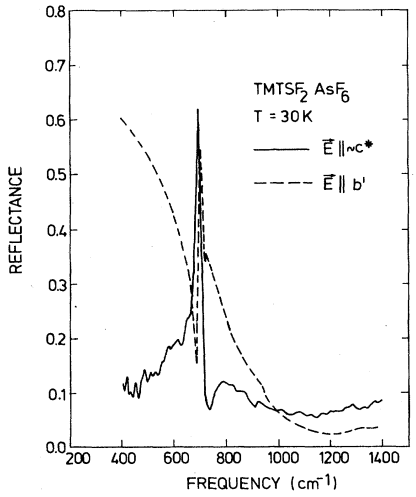

FIG. 8. Polarized reflectance for $\vec{E}||b'$ and $\vec{E}\sim||c^*$ of $(TMTSF)_2AsF_6$ at $T=30$ K. The frequency range is 400—1400 cm^{-1}.

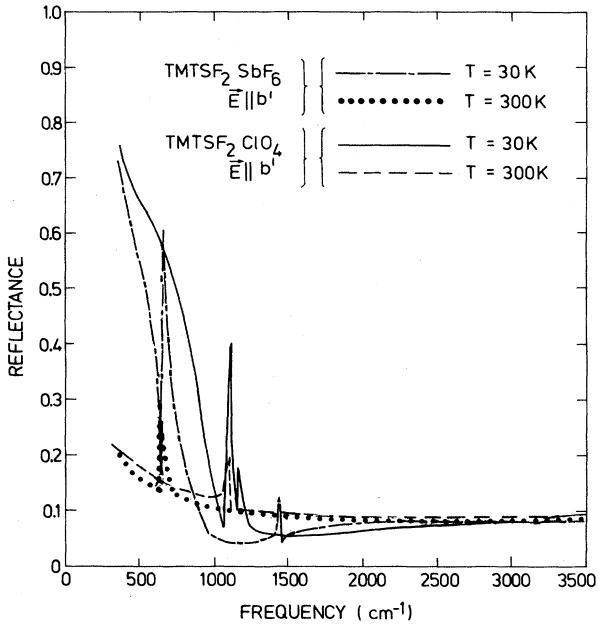

FIG. 9. Polarized reflectance for $\vec{E}||b'$ of $(TMTSF)_2SbF_6$ and $(TMTSF)_2ClO_4$ at $T=30$ and 300 K. The frequency range is 350—3500 cm^{-1}.

including extra oscillators. We have assumed the background dielectric constant to be the same, $\epsilon_\infty=3.5$, in all cases, as estimated from the reflectance level in the (3000—4000)-cm^{-1} range. Results based on room-temperature spectra show little change in oscillator strength, but are less accurate. In our earlier paper[17] we used a simple effective mass model to estimate the transfer integral from the plasma frequencies. As pointed out by Kwak,[43] the proper analysis also involves the chain axis transfer integral. For a simplified approach we consider a rectangular lattice with a tight-binding band

$$\epsilon(k_a,k_b)=2t_a\cos\left[k_a\frac{a}{2}\right]+2t_b\cos(k_b b)\ . \tag{5}$$

Assuming an open Fermi surface and $t_b \ll t_a$ we obtain from Eq. (2)

$$\omega_{p,b}^2 \cong \frac{2\sqrt{2}}{\pi}\frac{e^2b^2}{\epsilon_0\hbar^2V_m}\frac{t_b^2}{t_a}\ . \tag{6}$$

Thus apart from prefactors, the oscillator strength is suppressed by a factor of t_b/t_a. This is a result of the open Fermi surface, which produces many cancellations in the contributions to Eq. (2).

In Table II are given the resulting plasma frequencies and transfer integrals. Note that t_b correlates well with the b-axis lattice constant. Note also that $t_b\simeq 0.1t_a$ so that the assumption that $t_b \ll t_a$ may be questionable. However, the values given are in reasonable agreement with results from band-structure calculations reported by Grant.[44] The implied band-structure anisotropy varies from 15 in $(TMTSF)_2SbF_6$ to 12 in $(TMTSF)_2ClO_4$. It should be noted that the transverse bandwidths are of order 800—1100 K, so that the b-axis band curvature is significant at all temperatures of interest.

D. Chain-axis intraband excitations

Apart from slight shifts in the position of the plasma edge, the near-infrared chain-axis spectra of different materials look the same. As we shall see, this is not the case in the infrared region, where the effects of emv coupling and of metal-insulator transitions are evident.

The following materials will be discussed. (1) $(TMTSF)_2PF_6$ in its metallic phase, representing the highly conducting group of materials. (It was not possible to do measurements on this material below the metal-insulator transition at 12 K.) (2) $(TMTTF)_2PF_6$ as a typical example of a material with intermediate conductivity $[\sigma_a(300\text{ K})=20\ \Omega^{-1}cm^{-1}]$.[10] (3) $(TMTTF)_2Br$ which is

TABLE II. Drude parameters, transfer integrals, and b-axis lattice constant in $(TMTSF)_2X$, $\vec{E}||b'$.

X	ϵ_c	ω_p (cm^{-1})	Γ (cm^{-1})	t_b (meV)	b (Å)
ClO_4^-	3.50	2020	250	24	7.678 (Ref. 42)
SbF_6^-		1510	300	18	7.728 (Ref. 41)
AsF_6^-		1670	350	20	7.711 (Ref. 41)
PF_6^-		1830	500	22	7.711 (Ref. 13)

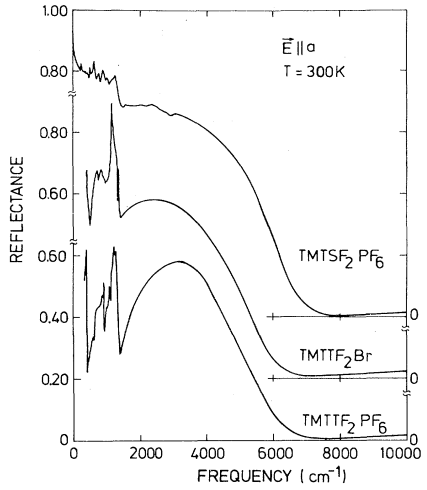

FIG. 10. Chain-axis reflectance of $(TMTSF)_2PF_6$, $(TMTTF)_2Br$, and $(TMTTF)_2PF_6$ at $T=300$ K. The frequency range is 10—10000 cm^{-1} for $(TMTSF)_2PF_6$, and 350—10000 cm^{-1} for the $(TMTTF)_2X$ salts.

the best metal in the $(TMTTF)_2X$ group [σ_a (300 K)$=260$ $\Omega^{-1}cm^{-1}$],[10] and which may be considered an intermediary between the two groups. Figure 10 shows the chain-axis polarized reflectance spectrum of these materials at 300 K. The main differences clearly appear below 3000 cm^{-1}, i.e., in the range of molecular vibrations. The material with lowest conductivity [$(TMTTF)_2PF_6$] has the strongest vibrational lines.

Figure 11 presents the frequency-dependent conductivities (determined by dispersion analysis[34]). The spectra can be viewed as broad peaks with fine structure of vibrational origin. These peaks are centered at 300, 1000, and 2200 cm^{-1} for $(TMTSF)_2PF_6$, $(TMTTF)_2Br$, and $(TMTTF)_2PF_6$, respectively. Thus there seems to be a correlation between the position of the broad band and the metallic quality, for example, measured by the dc conductivity. For an ideal metal [described by the Drude model, Eq. (1)], the electronic band is centered at zero frequency. We note that for the materials in Fig. 11 the $\sigma(\omega)$ curves can easily be extrapolated to the proper dc values.

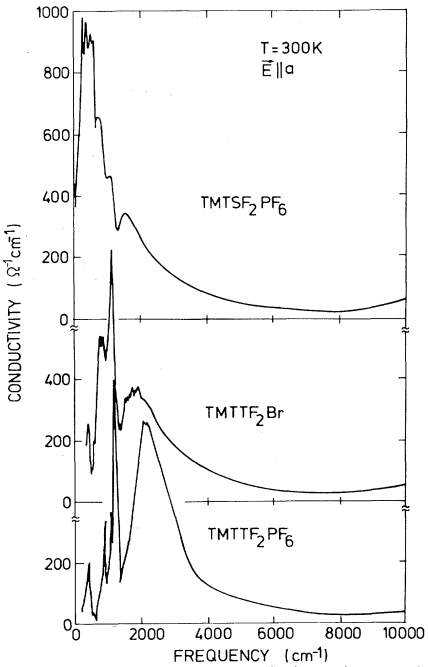

FIG. 11. Frequency-dependent chain-axis conductivity of $(TMTSF)_2PF_6$, $(TMTTF)_2Br$, and $(TMTTF)_2PF_6$ at $T=300$ K. The results are obtained by dispersion analysis of reflectance data. The frequency range is 10—10000 cm^{-1} for $(TMTSF)_2PF_6$, and 350—10000 cm^{-1} for the $(TMTTF)_2X$ salts.

The physics behind the shift of oscillator strength to higher frequencies is not well understood. It appears that Coulomb correlations play a role, i.e., they give rise to a partial localization of the wave functions (as in a Mott insulator); consequently oscillator strength shifts away from zero frequency. These ideas have been discussed qualitatively by Hubbard.[45] If, on the other hand, the electronic band is close to zero frequency, one may hope that models based on delocalized carriers [such as Eq. (2)] apply.

IV. ELECTRON-MOLECULAR-VIBRATION COUPLING EFFECTS

We will now turn to a discussion of the vibrational features. It is of value to include data on $(TMTSF)_2ReO_4$, which has a sharp metal-insulator transition at 183 K, related to anion ordering.[9] The reflectance and conductivity of $(TMTSF)_2ReO_4$ are shown in Fig. 12 for temperatures above and below the metal-insulator transition. Note that the low-temperature spectrum is similar to that of $(TMTTF)_2PF_6$ at 300 K, even though $(TMTSF)_2ReO_4$ at 40 K is believed to be an ordinary semiconductor, where the low conductivity is due to a gap at the Fermi level, caused by a $2k_F$ potential.[9]

Because most vibrational modes in the range of interest are polarized in the molecular plane, vibrational features polarized along the chain direction, i.e., almost perpendicular to this plane, are believed to be due to the Rice effect following from the emv coupling.[46,47] This coupling is nonzero only for the totally symmetric a_g modes and follows from the fact that the orbital energy levels in general will change when the size of the molecule is modulated.

A. Vibrational mode assignments

As basis for the discussion we list in Table III the calculated a_g modes for TMTSF, as given by Bozio *et al.*[21] We also include calculated coupling constants for the analogous modes in TTF^+,[48] where appropriate.

In addition we show $\sigma(\omega)$ for $(TMTSF)_2PF_6$ and $(TMTTF)_2PF_6$ (at 300 K), and $(TMTSF)_2ReO_4$ (at 40 K) on an expanded frequency scale in Fig. 13. $(TMTTF)_2PF_6$ and $(TMTSF)_2ReO_4$ both show a very strong resonance in the 1500-cm^{-1} range. This band is believed to be due to the (a_g,ω_4) mode[20,21] involving the central C=C stretches. As seen in Table III calculations indicate a large coupling to the electrons for this mode. It also clearly has the effect of producing a broad minimum in $\sigma(\omega)$ for $(TMTSF)_2PF_6$. Other modes which are of unambiguous

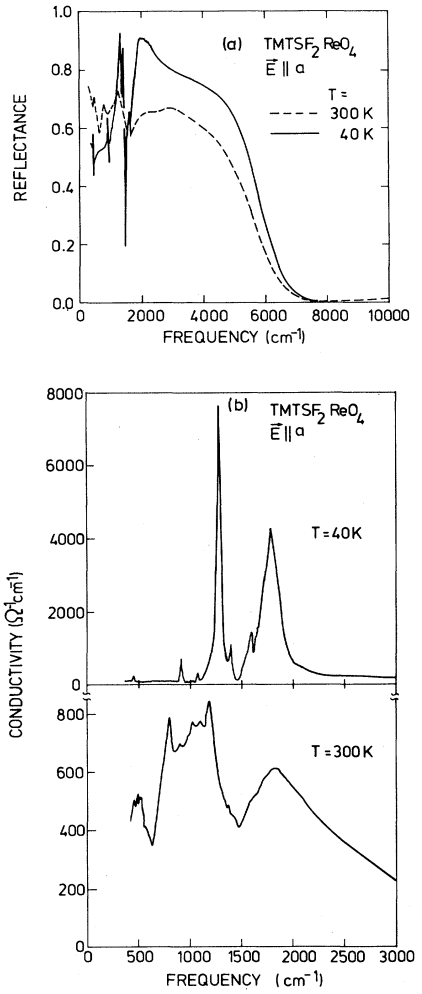

FIG. 12. Infrared properties of $(TMTSF)_2ReO_4$ above ($T=300$ K) and below ($T=40$ K) the metal-insulator transition at $T=183$ K. In (a) is shown the chain-axis reflectance in the range 400—10 000 cm^{-1}, and in (b) the resulting frequency-dependent conductivities in the range 400—3000 cm^{-1}. Notice the different conductivity scales at $T=300$ and 40 K.

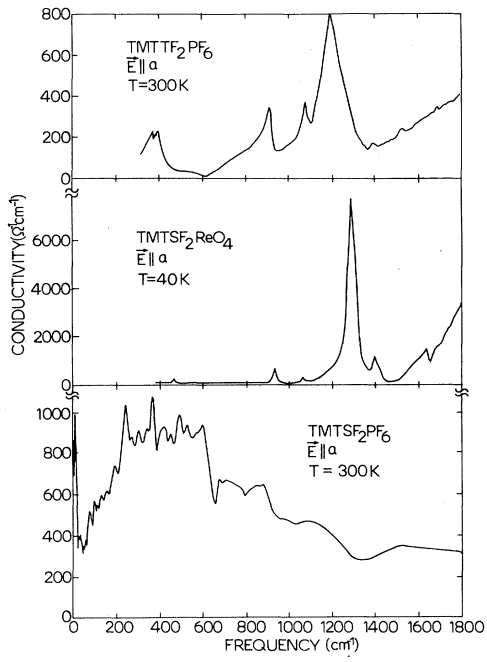

FIG. 13. Frequency-dependent chain-axis conductivity of $(TMTTF)_2PF_6$ and $(TMTSF)_2PF_6$ at $T=300$ K and of $(TMTSF)_2ReO_4$ at $T=40$ K. The lower-frequency limit is 350, 10, and 400 cm^{-1} for the three materials, respectively, and the upper limit 1800 cm^{-1}. Notice the different conductivity scales.

origin are the (a_g,ω_3) mode near 1600 cm^{-1}, only resolved in $(TMTSF)_2ReO_4$, the (a_g,ω_7) mode near 1100 cm^{-1}, and the (a_g,ω_9) mode at 430 cm^{-1} in $(TMTSF)_2ReO_4$. This latter mode involves the C—Se bond and the corresponding vibration should be at a somewhat higher frequency[20] in TMTTF (552 cm^{-1}), where it does not seem to be resolved. Finally the strong mode at 390 cm^{-1} in $(TMTTF)_2PF_6$ is the (a_g,ω_{10}) mode.[20]

Another mode, seen at 910 cm^{-1} in both materials, should be the (a_g,ω_8) mode involving the methyl groups. This assignment may safely be made in the case of $(TMTTF)_2PF_6$, since the line is almost completely polar-

TABLE III. A_g vibration modes for $TMTSF^0$ (Ref. 21).

No.	Calculated frequency (cm^{-1})	Dominating character	g_α for similar mode in TTF^+ (Ref. 48) (cm^{-1})
1	2954	C—H stretch	90
2	2862	C—H stretch	
3	1630	C=C stetch, central plus ring	360
4	1548	C=C stretch, central plus ring	940
5	1440	H—C—H bend	
6	1365	C—C—H, H—C—H bend	
7	1087	C—Se stretch, C—CH_3 stretch, C—C—H bend	
8	929	C—CH_3 stretch, C—C—H bend	
9	453	C—Se stretch, C—CH_3 stretch	360
10	299	C—Se stretch, ring deformation	630
11	240	Se—C—CH_3 bend	
12	146	C—Se stretch, ring deformation	40

ized along the chain axis (see Fig. 7, where it is absent). For $(TMTSF)_2ReO_4$ an assignment is less unambiguous, because ReO_4^- is known to have an absorption band very close to this positon.[21] However, because the ReO_4^- band is of comparable intensity to similar bands in PF_6^- at 835 cm^{-1}, and because these PF_6^- bands are only weakly seen in the chain-axis polarization in $(TMTTF)_2PF_6$, we conclude that most of the strength in the band is due to coupling with the (a_g,ω_8) mode. Furthermore, such a coupling may also account for the sudden drop in $\sigma(\omega)$ in $(TMTSF)_2PF_6$ at about the same frequency.

Similarly, the dip in the $(TMTSF)_2ReO_4$ spectrum at 1370 cm^{-1} may be due to coupling to the (a_g,ω_6) mode, which also involves the methyl groups. Bozio *et al.*[21] argue that this coupling constant should be very small, because little electron density is expected near the methyl groups, and suggest that the dip could be caused by anharmonic interaction between the fully symmetric modes. In our opinion the spectra can be taken as evidence for considerable electronic coupling to the methyl group modes. It follows that there must be a considerable charge density near the groups, and this observation may provide a clue to understanding the large difference in transfer integrals between TTF (TSF) and TMTTF (TMTSF).

B. Dimer model

A proper theory for the emv coupling effects in these materials does not exist. However, it turns out that a model based on isolated dimers describes the results rather well. It should just be kept in mind that the resulting parameters may have to be reinterpreted at a later stage. In the dimer theory[47] the dielectric function is described by

$$\tilde{\epsilon}(\omega)=\epsilon_\infty+\frac{\omega_p^2}{\omega_{CT}^2[1-D(\omega)]-\omega^2-i\omega\gamma_e}\ . \tag{7}$$

Here ω_p^2 is a measure of the strength in the charge-transfer band, ω_{CT} determines its position in the absence of vibrational coupling, γ_e is a relaxation rate, and ϵ_∞ is a background dielectric constant. The function $D(\omega)$ describes the modes and the coupling strengths:

$$D(\omega)=\sum_\alpha \frac{\lambda_\alpha\omega_\alpha^2}{\omega_\alpha^2-\omega^2-i\omega\gamma_\alpha}\ . \tag{8}$$

In Eq. (8), ω_α and γ_α, respectively, are the bare frequency and inverse lifetime of mode α, and λ_α is a dimensionless coupling constant. This quantity is related to the coupling constant g_α by

$$\lambda_\alpha=\frac{4\epsilon_0}{ne^2a^2}\frac{\omega_p^2}{\omega_{CT}^2}\frac{g_\alpha^2}{\omega_\alpha}\ , \tag{9}$$

where n is the dimer density, and a is the spacing between molecules.

We have fitted this model to the reflectance of $(TMTTF)_2PF_6$ at 300 K and $(TMTSF)_2ReO_4$ at 40 K. The quality of the fits may be seen in Figs. 14 and 15. The parameters found are listed in Table IV with the assignments described above.

Although the results look fairly reasonable, it seems

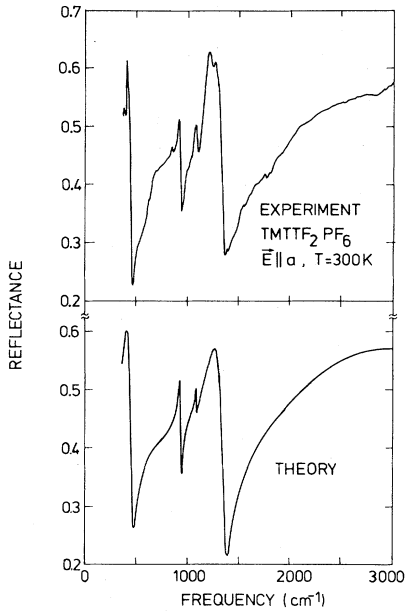

FIG. 14. Chain-axis reflectance of $(TMTTF)_2PF_6$ at $T=300$ K as measured and as calculated by fitting the dimer model to the data. The frequency range is 350—3000 cm^{-1}.

that both the predicted coupling constants and the frequency shifts are too small. For example, in $(TMTTF)_2PF_6$ the (a_g,ω_4) mode has $g_4=300$ cm^{-1} as compared with the calculated value of 940 cm^{-1} for TTF^+ (Table III). The mode is located at 1185 cm^{-1} and the bare frequency should be 1378 cm^{-1} according to Table IV. Torrance *et al.*[49] found by Raman spectroscopy

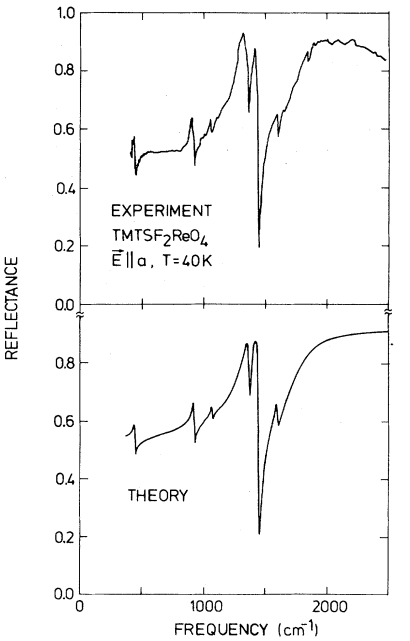

FIG. 15. Chain-axis reflectance of $(TMTSF)_2ReO_4$ at $T=40$ K as measured and as calculated by fitting the dimer model to the data. The frequency range is 400—2500 cm^{-1}.

TABLE IV. Dimer charge oscillator parameters for $(TMTTF)_2PF_6$ (300 K) and $(TMTSF)_2ReO_4$ (40 K).

	$(TMTTF)_2PF_6$ (300 K)			$(TMTSF)_2ReO_4$ (40 K)		
ω_p (cm^{-1})	8580			9800		
ω_{CT} (cm^{-1})	2220			1700		
γ_e (cm^{-1})	1460			300		
ϵ_∞	2.64			2.60		
Mode	ω_α (cm^{-1})	g_α (cm^{-1})	γ_α (cm^{-1})	ω_α (cm^{-1})	g_α (cm^{-1})	γ_α (cm^{-1})
a_g,ω_3				1600	36	17
a_g,ω_4	1378	300	71	1452	140	10
a_g,ω_6				1370	44	17
a_g,ω_7	1090	30	5	1062	16	10
a_g,ω_8	930	75	75	920	45	14
a_g,ω_9				444	41	14
a_g,ω_{10}	460	200	45			

that $\omega_4=1476$ cm^{-1} in another TMTTF compound with the same molecular charge. Bozio *et al.*[20] have also determined coupling constants from the dimer model. They base their calculation on the frequency shifts predicted by the dimer model, and therefore obtain somewhat different values: For $(TMTTF)_2BF_4$ they report $g_4=670$ cm^{-1} and $g_{10}=480$ cm^{-1}.

In conclusion we state that although the interpretation of the model described by Eq. (7) may be questioned, it seems clear that it describes the real spectra quite well. It is actually also possible by adjusting ω_{CT} to lower values to reproduce the qualitative features of, for example, the $(TMTTF)_2Br$ and $(TMTSF)_2PF_6$ spectra.

V. CHAIN-AXIS CONDUCTIVITY OF $(TMTSF)_2PF_6$

A. Results

We now turn to the a-axis properties of $(TMTSF)_2PF_6$ at three temperatures: 300, 100, and 25 K and concentrate on the range 0—1200 cm^{-1}. Figure 16 shows the reflectance starting at 10 cm^{-1}. Apart from the fine structure, most of which is unidentified, two features are remarkable. (1) R goes to unity at low frequencies in a non-Drude manner. The Drude model predicts $1-R\sim\sqrt{\omega}$ for $\omega\ll\Gamma$, while we find in the low-temperature data a reflectance near unity extending to 20 cm^{-1} and then a sudden drop to 80—82 %. (2) The 25- and 100-K reflectance rises again at higher frequencies. At 25 K there is a range from 400 to 900 cm^{-1} where R is 95—99 %.

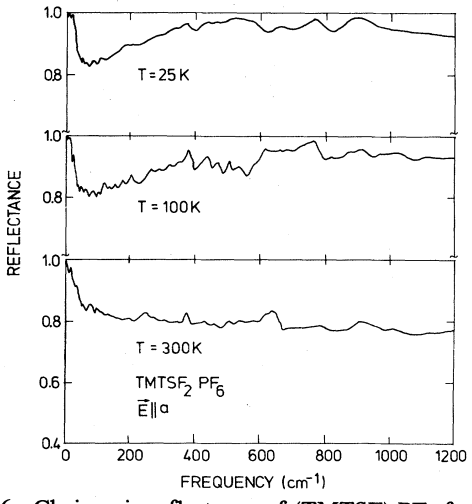

FIG. 16. Chain-axis reflectance of $(TMTSF)_2PF_6$ for $T=25$, 100, and 300 K. The frequency range is 10—1200 cm^{-1}.

These features have important consequences for the frequency-dependent conductivity and dielectric function, which we have calculated by dispersion analysis, and present in Figs. 17 and 18. The basic features are clear:

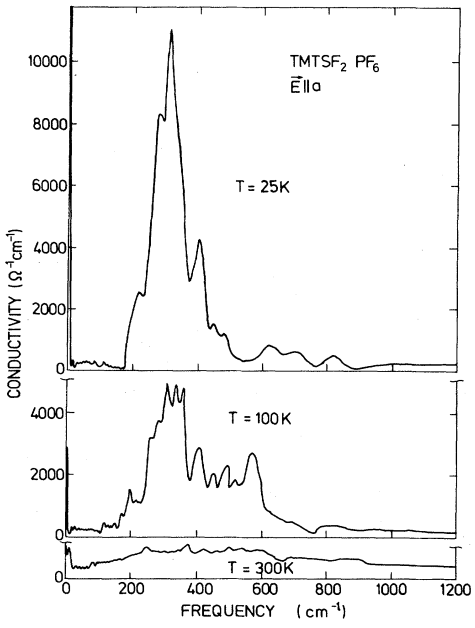

FIG. 17. Frequency-dependent chain-axis conductivity of $(TMTSF)_2PF_6$ for $T=25$, 100, and 300 K. The results are obtained by dispersion analysis of reflectance data. The valid frequency range is 10—1200 cm^{-1}. However, the curves are extrapolated towards the known dc values below 10 cm^{-1}.

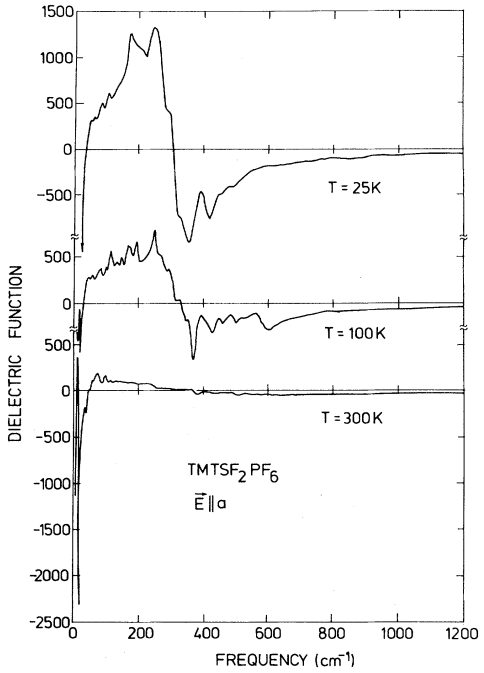

FIG. 18. Real part of the chain-axis dielectric function of $(TMTSF)_2PF_6$ for $T=25$, 100, and 300 K. The results are obtained by dispersion analysis of reflectance data. The frequency range is 10—1200 cm^{-1}.

A dominant peak in $\sigma_a(\omega)$ around 300 cm^{-1} grows up with decreasing temperature. This growth is accompanied by a suppression of the far-infrared conductivity. The upturn towards the dc values indicated in Fig. 17 is implied by, but not contained in the data. At 25 K there is virtually an excitation gap up to 180 cm^{-1}. The distribution of oscillator strength [i.e., the area under the $\sigma_a(\omega)$ curves] can be estimated from the data. At 25 K about 70% of the total strength (as given by ω_p) is contained in the 300-cm^{-1} peak. Furthermore, it is possible to make a reasonable estimate of the strength in the narrow mode near dc, if $\tilde{\epsilon}(\omega)$ is modeled as a sum of three terms:

$$\tilde{\epsilon}(\omega)=\epsilon_\infty+\frac{\beta\omega_p^2}{\omega_0^2-\omega^2-i\omega\Gamma}-\frac{\Omega_p^2}{\omega(\omega+i\gamma)}\ , \tag{10}$$

where the second and the third terms represent the dominant peak and the narrow mode, respectively.

At 25 K, $\beta=0.70$ (see above) and $\omega_o\cong 300$ cm^{-1}. Thus at 31 cm^{-1}, where $\epsilon_1(\omega)$ crosses zero (see Fig. 18), the first two terms represent an approximately frequency-independent background dielectric constant of about 800. The last term will cancel this contribution at 31 cm^{-1} for $\Omega_p\cong 900$ cm^{-1}. Finally with[3] $\sigma_{dc}(25\ K)=5\times 10^4$ $\Omega^{-1}cm^{-1}$, the halfwidth γ may be estimated to 0.3 cm^{-1}, which corresponds roughly to 10 GHz. Thus the results indicate that $\sigma(\omega)$ should fall rather rapidly through the microwave range. 35-GHz data[3] do in fact yield a somewhat higher resistivity than dc data in this temperature range, and perhaps more significantly, $\sigma_{35\ GHz}$ increases more slowly with decreasing temperature below 50 K than does σ_{dc}.

B. Background

In order to interpret the data, it is useful to describe shortly the far-infrared properties of other highly conducting organics. The far-infrared properties of $(TMTSF)_2ClO_4$ have recently been measured by Ng *et al.*[23] and by Challener *et al.*[24] $(TMTSF)_2ClO_4$ has no metal-insulator transition, but rather a superconducting transition at 1.3 K.[5] The reflectance at helium temperatures is high (96—99 %) up to 30 cm^{-1} and then falls abruptly to 90%. Although this behavior is somewhat similar to $(TMTSF)_2PF_6$, there is considerable structure below 30 cm^{-1}: $\sigma_a(\omega)$ displays a double-peak structure which, however, rapidly disappears with increasing temperature. With the applied extrapolations $\sigma_a(\omega)$ rises gradually from a minimum at 30 cm^{-1} on going to higher frequencies. Thus the sudden increase in $(TMTSF)_2PF_6$ at 180 cm^{-1} is absent.

The far-infrared conductivity of TTF-TCNQ (Ref. 27) at the conductivity maximum ($T=60$ K) also shows some similarities with that of $(TMTSF)_2PF_6$. There is a peak in $\sigma(\omega)$ at 300 cm^{-1}, usually attributed to a fluctuating Peierls gap,[27] a rather low conductivity in the (20—200)-cm^{-1} range, and then a rise towards the dc value. The low-frequency rise is thought to be due to charge-density-wave contributions to the conductivity.

C. Spin-density-wave model

Returning to the $(TMTSF)_2PF_6$ data, a comparison with $(TMTSF)_2ClO_4$ hints that the difference in the far-infrared properties is related to the known differences in physical properties: $(TMTSF)_2ClO_4$ is known to have less tendency towards a spin-density-wave (SDW) instability than $(TMTSF)_2PF_6$, where a SDW ordered state is found below 12 K.[6] Thus we may assume that the observed gap is a threshold for SDW excitations. These should have a sharp gap[50] as observed. Under this assumption, the behavior is analogous to that of TTF-TCNQ: The narrow contribution to $\sigma(\omega)$ at dc is due to current carrying, sliding SDW's (Ref. 51) and the single-particle contributions are suppressed by a pseudogap, originating from the spin-density waves. These SDW's have a wave vector which just spans the Fermi surface. This interpretation assumes that there are important SDW fluctuations above the actual transition temperature. In spite of the rather large b-axis transfer integral, the fluctuations appear to be rather one dimensional: The absence of a pseudogap along b' (cf. Fig. 6) suggests that the transverse correlation length is limited to a few lattice constants.

That magnetic order may exist in the conducting state in these materials is independently confirmed by the observation of antiferromagnetic resonance in $(TMTSF)_2ClO_4$.[52] This shows that a SDW structure may be present without suppressing the dc conductivity. In a sense we are speaking about an itinerant antiferromagnet. But the real antiferromagnetism as detected in the macroscopic susceptibility[6] does not occur until full three-dimensional order is established.

Pursuing the idea of important SDW fluctuations we may estimate the amplitude of the SDW's from the gap

size, using the simplest possible mean-field theory, which predicts[53]

$$E_g = 2\epsilon_F \exp[-1/\rho_\uparrow(\epsilon_F)\tilde{U}] = 2\frac{\mu}{\mu_B}\tilde{U} . \quad (11)$$

Here μ/μ_B is the amplitude (as fraction of the Bohr magneton), $\rho_\uparrow(\epsilon_F)$ is the single-spin density of states at the Fermi level ϵ_F, and $\tilde{U}$ is an effective Coulomb repulsion. With $t_a = 0.28$ eV we have $\epsilon_F = 0.16$ eV and $\rho_\uparrow(\epsilon_F) = 0.80$ eV^{-1}. The observed gap at 180 cm^{-1} corresponds to $E_g = 22$ meV. Then Eq. (8) gives $\tilde{U} = 0.47$ eV and $\mu/\mu_B = 2.3\%$. Other estimates of μ/μ_B span this value, ranging from[7] 0.6% to[8] 10–20%.

Finally we note that $E_g = 22$ meV is the direct, optical gap. The observed thermodynamic gap of 4 meV (Ref. 54) in the semiconducting state indicates that below 12 K, the SDW wave vector does not nest the full Fermi surface. Incomplete nesting has been discussed in detail by Kwak[55] in connection with the occurence of quantum oscillations. In view of the large transverse coupling, it will lead to a considerable reduction of the thermodynamic gap, even if the direct gap is unchanged.

V. CONCLUSIONS

In summary, we have made extensive measurements of the optical properties of $(TMTSF)_2X$ and $(TMTTF)_2X$ compounds. The data have been analyzed to obtain information about the electronic properties of these materials.

We have obtained three independent indications that the highest occupied molecular orbital on $(TMTSF)^0$ or $(TMTSF)^+$ differs qualitatively from the corresponding TTF and TSF orbital: (1) The visible spectrum shows new structure, (2) the chain-axis transfer integral is unusually large ($t_a \cong 0.25$ eV at 300 K) for a slipped overlap, and (3) the anomalous emV spectra indicate considerable charge density near the methyl groups. This latter conclusion also holds for TMTTF.

The chain-axis infrared spectra for a series of compounds in the $(TMTSF)_2X$ and $(TMTTF)_2X$ family show a charge-transfer band. The position of this band correlates with the metallic character: a low-peak position corresponds to a high-dc conductivity. The vibronic features can be modeled very well using a simple dimer charge oscillator model.

The conducting $(TMTSF)_2X$ compounds display the unique feature of a b-axis plasma edge near 1000 cm^{-1}. Bandwidth anisotropies are found to be in the range 12–15 for different materials, and indicate open Fermi surfaces with significant two-dimensional character.

Finally, in $(TMTSF)_2PF_6$ the charge-transfer band is centered at 300 cm^{-1} and sharpens up with decreasing temperature. At 25 K a virtual gap appears at 180 cm^{-1}. This gap is interpreted as an onset of excitations in a spin-density-wave structure, and implies that the dc conductivity is dominated by spin-density-wave transport. Analysis suggests a small-amplitude spin-density wave of $0.02\mu_B$ at 25 K.

ACKNOWLEDGMENTS

We acknowledge informative discussions with J. B. Torrance, T. Timusk, R. Bozio, and P. M. Grant. We thank I. Johannsen for supplying the $(TMTTF)_2Br$ crystals. The collaborative aspect of the work has been supported by the NATO Research Grants Programme. One of us (C.S.J.) acknowledges support from the Danish Natural Science Research Council and from the Royal Danish Academy of Sciences and Letters through a Niels Bohr Scholarship.

[1]Proceedings of the International Conference on Low Dimensional Conductors, Boulder, Colorado, 1981 [Mol. Cryst. Liq. Cryst. 77 (1981); 79, 81, 83, 85, 86 (1982)].

[2]Proceedings of the International Conference on Low Dimensional Conductors and Superconductors, Les Arcs, 1982 [J. Phys. (Paris) Colloq. 3 (1983)].

[3]K. Bechgaard, C. S. Jacobsen, K. Mortensen, H. J. Pedersen, and N. Thorup, Solid State Commun. 33, 1119 (1980).

[4]D. Jerome, A. Mazaud, M. Ribault, and K. Bechgaard, J. Phys. (Paris) Lett. 41, L95 (1980).

[5]K. Bechgaard, K. Carneiro, M. Olsen, F. B. Rasmussen, and C. S. Jacobsen, Phys. Rev. Lett. 46, 852 (1981).

[6]K. Mortensen, Y. Tomkiewicz, T. D. Schultz, and E. M. Engler, Phys. Rev. Lett. 46, 1234 (1981).

[7]A. Andrieux, D. Jerome, and K. Bechgaard, J. Phys. (Paris) Lett. 42, L87 (1981).

[8]J. B. Torrance, H. J. Pedersen, and K. Bechgaard, Phys. Rev. Lett. 49, 881 (1982).

[9]C. S. Jacobsen, H. J. Pedersen, K. Mortensen, G. Rindorf, N. Thorup, J. B. Torrance, and K. Bechgaard, J. Phys. C 15, 2651 (1982).

[10]P. Delhaes, C. Coulon, J. Amiell, S. Flandrois, E. Toreilles, J. M. Fabre, and L. Giral, Mol. Cryst. Liq. Cryst. 50, 43 (1979).

[11]S. S. P. Parkin, F. Creuzet, M. Ribault, D. Jerome, K. Bechgaard, and J. M. Fabre, Mol. Cryst. Liq. Cryst. 79, 249 (1982).

[12]J. P. Pouget, R. Moret, R. Comes, and K. Bechgaard, J. Phys. (Paris) Lett. 42, L543 (1981).

[13]N. Thorup, G. Rindorf, H. Soling, and K. Bechgaard, Acta Crystallogr. Sect. B 37, 1236 (1981).

[14]B. Liautard, S. Peytavin, G. Brun, and M. Maurin, J. Phys. (Paris) 43, 1454 (1982).

[15]T. J. Kistenmacher, T. E. Phillips, and D. O. Cowan, Acta Crystallogr. Sect. B 30, 763 (1974).

[16]V. J. Emergy, R. Bruinsma, and S. Barisic, Phys. Rev. Lett. 48, 1039 (1982).

[17]C. S. Jacobsen, D. B. Tanner, and K. Bechgaard, Phys. Rev. Lett. 46, 1142 (1981).

[18]C. S. Jacobsen, D. B. Tanner, and K. Bechgaard, Mol. Cryst. Liq. Cryst. 79, 25 (1982); J. Phys. (Paris) Colloq. 3, C-859 (1983).

[19]K. Kikuchi, Y. Ikemoto, K. Yakushi, H. Kuroda, and K. Kobayashi, Solid State Commun. 42, 433 (1982).

[20]R. Bozio, M. Meneghetti, and C. Pecile, J. Chem. Phys. 76, 5785 (1982).

[21]R. Bozio, C. Pecile, K. Bechgaard, F. Wudl, and D. Nalewa-

jek, Solid State Commun. 41, 905 (1982).
[22]H. K. Ng, T. Timusk, J. M. Delrieu, D. Jerome, K. Bechgaard, and J. M. Fabre, J. Phys. (Paris) Lett. 43, L513 (1982).
[23]H. K. Ng, T. Timusk, and K. Bechgaard, J. Phys. Paris Colloq. 3, C-867 (1983).
[24]W. A. Challener, P. L. Richards, and R. L. Greene, J. Phys. Paris Colloq. 3, C-873 (1983).
[25]H. W. Helberg, J. Phys. Paris Colloq. 3, C-1021 (1983).
[26]L. B. Coleman, Ph.D. thesis, University of Pennsylvania,1975 (unpublished).
[27]D. B. Tanner and C. S. Jacobsen, Mol. Cryst. Liq. Cryst. 85, 137 (1982).
[28]P. M. Grant, R. L. Greene, G. C. Wrighton, and G. Castro, Phys. Rev. Lett. 31, 1311 (1973).
[29]R. Zahradnik, P. Carsby, S. Hünig, G. Kiesslich, and D. Scheutzow, Int. J. Sulfur Chem. C 6, 109 (1971).
[30]R. Gleiter, M. Kobayashi, J. Spanget-Larsen, J. P. Ferraris, A. N. Bloch, K. Bechgaard, and D. O. Cowan, Ber. Bunsenges. Phys. Chem. 79, 1218 (1975).
[31]J. B. Torrance, B. A. Scott, B. Welber, F. B. Kaufman, and P. E. Seiden, Phys. Rev. B 19, 730 (1979).
[32]T. Sugano, K. Yakushi, and H. Kuroda, Bull. Chem. Soc. Jpn. 51, 1041 (1978).
[33]Y. Cao, K. Yakushi, and H. Kuroda, Solid State Commun. 35, 739 (1980).
[34]F. Wooten, *Optical Properties of Solids* (Academic, New York, 1972).
[35]K. Mortensen, Solid State Commun. 44, 643 (1982).
[36]C. S. Jacobsen (unpublished).
[37]S. Etemad, T. Penney, E. M. Engler, B. A. Scott, and P. E. Seiden, Phys. Rev. Lett. 34, 741 (1975).
[38]B. Welber, P. E. Seiden, and P. M. Grant, Phys. Rev. B 18, 2692 (1978).
[39]G. M. Begun and A. C. Rutenberg, Inorg. Chem. 6, 2212 (1967).
[40]C. S. Jacobsen, K. Mortensen, M. Weger, and K. Bechgaard, Solid State Commun. 38, 423 (1981).
[41]N. Thorup (unpublished).
[42]K. Bechgaard, K. Carneiro, F. B. Rasmussen, M. Olsen, G. Rindorf, C. S. Jacobsen, H. J. Pedersen, and J. C. Scott, J. Am. Chem. Soc. 103, 2440 (1981).
[43]J. F. Kwak, Phys. Rev. B 26, 4789 (1982).
[44]P. M. Grant, Phys. Rev. B 26, 6888 (1982).
[45]J. Hubbard, Phys. Rev. B 17, 494 (1978).
[46]M. J. Rice, Phys. Rev. Lett. 37, 36 (1976); Solid State Commun. 31, 93 (1979).
[47]M. J. Rice, V. M. Yartsev, and C. S. Jacobsen, Phys. Rev. B 21, 3437 (1980).
[48]N. O. Lipari, M. J. Rice, C. B. Duke, R. Bozio, A. Girlando, and C. Pecile, Int. J. Quantum Chem. Symp. 11, 583 (1977).
[49]J. B. Torrance, J. J. Mayerle, V. Y. Lee, R. Bozio, and C. Pecile, Solid State Commun. 38, 1165 (1981).
[50]E. W. Fenton and G. C. Psaltakis, Solid State Commun. 47, 767 (1983).
[51]P. A. Lee, T. M. Rice, and P. W. Anderson, Solid State Commun. 14, 703 (1974).
[52]W. M. Walsh, Jr., F. Wudl, E. Aharon-Shalom, L. W. Rupp. Jr., J. M. Vandenburg, K. Andres, and J. B. Torrance, Phys. Rev. Lett. 49, 885 (1982).
[53]J. C. Scott, Mol. Cryst. Liq. Cryst. 79, 49 (1982).
[54]P. M. Chaikin, P. Haen, E. M. Engler, and R. L. Greene, Phys. Rev. B 24, 7155 (1981).
[55]J. F. Kwak, Phys. Rev. B 28, 3277 (1983).